Compressibility and strength of nanocrystalline tungsten boride under compression to 60GPa

Haini Dong, Susannah M. Dorfman, Ying Chen, Haikuo Wang, Jianghua Wang et al.

Citation: J. Appl. Phys. **111**, 123514 (2012); doi: 10.1063/1.4728208
View online: http://dx.doi.org/10.1063/1.4728208
View Table of Contents: http://jap.aip.org/resource/1/JAPIAU/v111/i12
Published by the American Institute of Physics.

Compressibility and strength of nanocrystalline tungsten boride under compression to 60 GPa

Haini Dong,[1,2] Susannah M. Dorfman,[2] Ying Chen,[1] Haikuo Wang,[1] Jianghua Wang,[1] Jiaqian Qin,[3] Duanwei He,[1,a)] and Thomas S. Duffy[2,a)]
[1]*Institute of Atomic and Molecular Physics, Sichuan University, Chengdu 610065, China*
[2]*Department of Geosciences, Princeton University, Princeton, New Jersey 08544, USA*
[3]*Geodynamics Research Center, Ehime University Bunkyo-cho 2-5, Matsuyama 790-8577, Japan*

(Received 1 March 2012; accepted 8 May 2012; published online 21 June 2012)

The compression behavior and stress state of nanocrystalline tungsten boride (WB) were investigated using radial x-ray diffraction (RXRD) in a diamond-anvil cell under non-hydrostatic compression up to 60.4 GPa. The compression properties and stress state are analyzed using lattice strain theory. Experiments were conducted at beamline X17C of the National Synchrotron Light Source. The radial x-ray diffraction data yield a bulk modulus that is qualitatively consistent with density functional theory calculations and demonstrate that WB is a highly incompressible material. A maximum differential stress, t, of about 14 GPa can be supported by nanocrystalline WB at the highest pressure. This corresponds to about 5% of the shear modulus, G, which is smaller than the values of t/G (~8%–10%) observed for BC_2N, B_6O, TiB_2, and γ-Si_3N_4 at high pressures. Thus, while WB is highly incompressible, its strength is relatively low at high pressures compared to other hard ceramics. © *2012 American Institute of Physics*. [http://dx.doi.org/10.1063/1.4728208]

INTRODUCTION

There has been recent interest in transition metal borides (TMs) as potential new avenues for synthesizing hard materials.[1–4] Tungsten borides, WB_x, which include WB, WB_2, and WB_4 and are analogous to tungsten carbides, have been reported to have numerous useful physical and chemical characteristics.[3,5–8] Tungsten boride, WB, has a Vickers hardness of about 28 GPa.[3] It combines high hardness with high heat resistance, good wear resistance, and high electrical resistance at high temperatures.[9–12] These attributes make tungsten boride attractive for potential abrasive, corrosion-resistant, and high-temperature applications.[3] Moreover, a comparative study[13] between WB polycrystalline compacts and WC-8 wt. % Co composites confirmed that WB and its composite materials have potential as new hard alloy tools for industrial use. Despite its potential applications, the high-pressure behavior of WB is poorly characterized. WB has not been investigated to date under static compression. Chen *et al.*[13] determined the elastic properties of polycrystalline WB compacts using ultrasonic methods at ambient conditions. The bulk modulus (K), shear modulus (G), and Young's modulus (Y) were determined to be $K = 266.9$ GPa, $G = 178.3$ GPa, $Y = 437.5$ GPa.[13] In contrast, theoretical studies[5,6] using first principles methods predicted much higher elastic moduli ($K = \sim 350$ GPa, $G = \sim 220$ GPa, and $Y = \sim 550$ GPa).

In order to determine its compressive behavior and mechanical properties, we performed a compression study on nanocrystalline WB up to 60.4 GPa in a diamond anvil cell using angle-dispersive x-ray diffraction in a radial geometry.[14–17] Radial x-ray diffraction together with lattice strain theory[14,18,19] enables us to measure the variation of the lattice strain at any orientation with respect to the loading axis and to obtain constraints on the compression behavior and the equation of state. From the analysis of lattice strains, we can determine the differential stress supported by the sample. This approach enables us to characterize both compressibility and shear strength.[20–22]

THEORETICAL BACKGROUND

The stress state in a polycrystalline sample under uniaxial loading in a diamond anvil cell is characterized by a maximum stress along the DAC loading axis, σ_3, and a minimum stress in the radial direction, σ_1. The difference between σ_3 and σ_1 is the macroscopic differential stress, t. Lattice strain theory[14,18,19,23,24] relates stress conditions to differences in lattice strain as a function of orientation relative to the compression axis and crystal anisotropy. The measured d-spacing (d_m) is a function of the angle ψ between the DAC loading axis and the diffraction plane normal and diffraction plane (hkl)

$$d\mathrm{m}(hkl) = d_p(hkl)[1 + (1 - 3\cos^2\psi)Q(hkl)], \quad (1)$$

where $d_p(hkl)$ is the d spacing under the mean normal stress $\sigma_p = (2\sigma_1 + \sigma_3)/3$ and $Q(hkl)$ is the orientation dependent lattice strain[23,24]

$$Q(hkl) = t/[6G^X(hkl)]. \quad (2)$$

$G^X(hkl)$ is the diffraction shear modulus for the (hkl) lattice planes, which is given by

$$[G^{\mathrm{X}}(hkl)]^{-1} = \left\{\alpha\left[G_{\mathrm{R}}^{\mathrm{X}}(hkl)\right]^{-1} + (1-\alpha)[G_{\mathrm{V}}(hkl)]^{-1}\right\}. \quad (3)$$

a)Authors to whom correspondence should be addressed. Electronic addresses: duanweihe@scu.edu.cn and duffy@princeton.edu.

$G_R^X(hkl)$ is the diffraction shear modulus assuming stress continuity (Reuss limit) across the grain boundaries and G_V denotes the aggregate shear modulus under strain continuity (Voigt bound) across the interfaces between the crystallites, respectively. α is the parameter specifying the degree of stress and strain continuity across grains in the polycrystalline sample. While normally the value of α is considered to be between 0.5 and 1, recently it has been shown that the value of α can be greater than 1 for materials for which the elastic anisotropy, $x = 2C_{44}/(C_{11} - C_{12})$, is less than one.[24,25] Equation (1) indicates a linear relation between d_m and $1 - 3\cos^2\psi$. The intercept, $1 - 3\cos^2\psi = 0$, is the d-spacing at $\psi = 54.7°$, which corresponds to d_p. Thus the hydrostatic compression curve can be estimated from the diffraction data at $\psi = 54.7°$. The slope of the fit yields the product $d_p(hkl)Q(hkl)$. The differential stress of the sample can be given by[14,19]

$$t = 6G\langle Q(hkl)\rangle f(x), \tag{4}$$

where $\langle Q(hkl)\rangle$ represents the average value of $Q(hkl)$ over all observed peaks and G is the aggregate shear modulus of a randomly oriented polycrystalline sample. f is a function of α and the elastic anisotropy parameter, x, which is close to 1 over a wide range of α and x values.[14,24,25] This method has been applied successfully to a large number of materials.[13,14,16,17,19–21]

EXPERIMENTS

Nanocrystalline tungsten boride (WB) was synthesized at 3 GPa and 1000 °C in a large volume press[3] from a 1:1 molar mixture of tungsten and boride. The WB nanocrystals (average grain size ~37 nm as determined from high-resolution transmission electron microscopy) have a tetragonal structure (space group $I4_1/amd$ No.141) with lattice parameters $a = 3.114$ Å and $c = 16.932$ Å. The sintered sample was ground to a powder and then loaded into a 100-μm-diameter hole in a beryllium gasket in a diamond anvil cell. The gasket was pre-indented to ~30-μm thickness. A piece of ~20-μm-diameter W foil was placed on top of the sample within ~5 μm of the sample centre to serve as a pressure marker as well as the sample position reference. A symmetric diamond anvil cell with a culet size of 300 μm was used to compress the sample. By design, no pressure medium was used thereby creating non-hydrostatic conditions in the sample chamber.

Angle dispersive x-ray diffraction in a radial geometry[14–17] was performed at the X17C beam line of National Synchrotron Light Source at Brookhaven National Laboratory. The diamond anvil cell was oriented with the incoming x-ray beam perpendicular to the diamond axis and passing through the Be gasket. The x-ray beam had a wavelength 0.3768 Å and was focused to 25 μm × 30 μm using Kirkpatrick-Baez mirrors. The diffracted intensity was recorded with a Rayonix SX-165 CCD detector. The 2D diffraction images were analyzed with the program FIT2D (Ref. 26) after calibration of the detector distance and orientation using a CeO_2 standard.

Diffraction patterns were collected at steps of ~5 GPa. After each pressure increase, sufficient time was allowed for stress relaxation prior to collection of the x-ray diffraction patterns. The (004), (101), (103), (105), (112), (008), (107), (116), and (200) diffraction peaks of WB were visible through the entire experimental range, but the (112), (008), (116), and (200) diffraction peaks were overlapped for all or part of the pressure range so these peaks were not used for lattice parameter determination or in the lattice strain analysis. The pressures were derived from the equation of state of W (Ref. 27) using the unit cell volume obtained from the (111) peak of W.

RESULTS AND DISCUSSION

In order to determine the variation in the positions of the diffraction peaks with the azimuthal angle, δ, the diffraction patterns were cut into small arcs of 3° to 5° intervals, in steps from 0° to 90° and integrated with FIT2D. Figure 1 presents representative diffraction patterns at 46.1 GPa at selected δ. The azimuthal angle is defined as zero in the maximum strain direction along the loading axis.[16] The diffraction peaks shift to larger diffraction angle 2θ at smaller δ corresponding to smaller d spacing in the maximum stress direction. Diffraction peak positions were fitted individually with Voigt line shapes and a linear background. The pole distance, ψ, is calculated from $\cos\psi = \cos\theta\cos\delta$.[16] Figure 2 shows the variation of d-spacing of the 103 line of WB versus $(1 - 3\cos^2\psi)$ which yields the expected linear variation. The increase in slope with pressure reflects the increase in $Q(103)$ resulting from the increase in differential stress, t, with compression.

Figure 3 shows the volume-pressure relation at $\psi = 0°$, 54.7°, and 90°, respectively. At $\psi = 0°$ and 90°, the lattice parameters show maximum and minimum lattice strain, respectively.[14,18,19] According to Eq. (1), the hydrostatic lattice parameters can be determined from the d-spacings at $(1 - 3\cos^2\psi) = 0$ ($\psi = 54.7°$).[14] The hydrostatic pressure is determined from the lattice parameter of W at $\psi = 54.7°$ together with its equation of state.[27] The compression curves are fitted

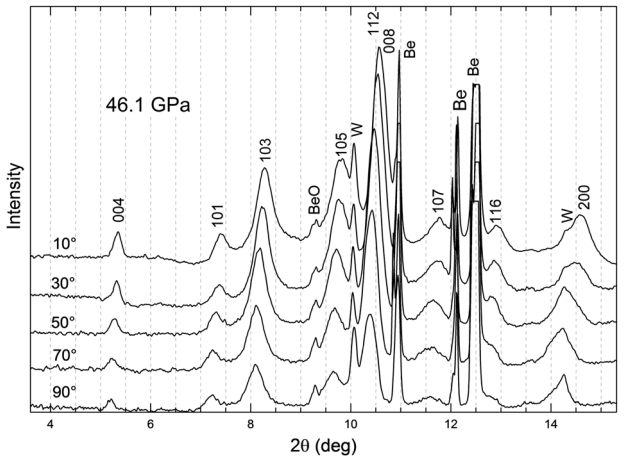

FIG. 1. Representative diffraction patterns at different azimuthal angles, δ, for WB at 46.1 GPa. Diffraction peaks of WB (with hkl), W, Be, and BeO are labeled in the figure.

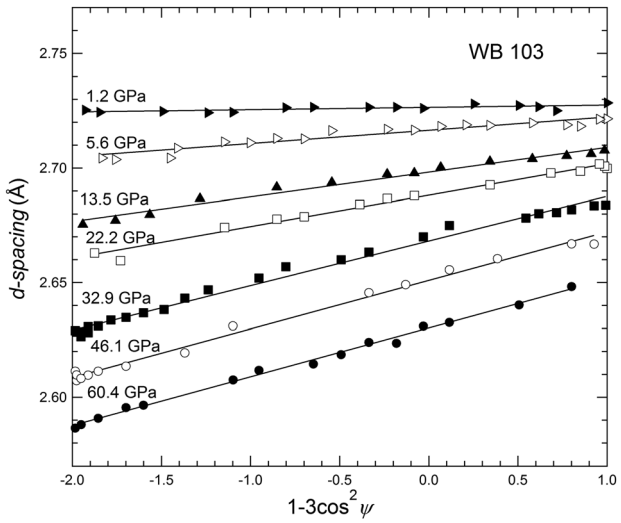

FIG. 2. Dependence of observed d spacing vs. 1-3cos$^2\psi$ for the (103) diffraction line of WB at selected pressures. The solid lines are least-squares fits to the data.

to the third-order Birch-Murnaghan equation of state, which yields the bulk modulus and its pressure derivatives at the three diffraction angles. The compression curve at $\psi = 54.7°$ yields a zero-pressure bulk modulus $K_0 = 417 \pm 18$ GPa, and a pressure derivative $K'_0 = 4.6 \pm 1.1$. The fitted results together with values from other work are listed in Table I. The hydrostatic zero-pressure bulk modulus obtained at $\psi = 54.7°$ in this work is much higher than that of the bulk sample from the previous ultrasonic study.[13] The bulk modulus we have determined is closer to but still larger than the results from theoretical studies using density functional theory.[5,6] The high bulk modulus of our WB sample may be enhanced by the nanocrystalline grain size of the sample.[28–33] While the effects of grain size on compressibility is complex, an enhanced bulk

TABLE I. A summary of the bulk modulus of WB and its pressure derivative from this work and published values.

K_0 (GPa)	K_0'	Reference
417 ± 18	4.6 ± 1.1	This study XRD $\psi = 54.7°$
428 ± 4	4.0 (fixed)	This study XRD $\psi = 54.7°$
267 ± 1		Ultrasonic (Ref. 13)
360		Density functional theory (Ref. 5)
375		Density functional theory (Ref. 6)

modulus in nanomaterials has been observed previously[28,34] and may be consistent with a core-shell model.[30–32] However, other materials do not show compressibility dependence on the grain size.[35–38] In addition, based on previous studies using this technique,[15,20,22] the equation of state at $\psi = 54.7°$ in the radial geometry may overestimate the value of K_0 due to local deviatoric stresses which would invalidate the assumption of uniaxial stress required for Eq. (1).[39,40] For more precise determination, it is necessary to follow-up with experiments under hydrostatic or quasi-hydrostatic conditions. Nevertheless, our results provide empirical support for the theoretical calculations that indicate that the bulk modulus is greater than 350 GPa, and thus WB is a highly incompressible solid. For WB, the *a* axis is slightly more compressible than the *c* axis and the *c/a* ratio remains nearly constant with increasing pressure. The variation of relative lattice parameters with pressure at $\psi = 54.7°$ is shown in the inset of Fig. 3. The linear incompressibilities are 406 GPa (K_a) and 445 GPa (K_c), respectively, from an equation of state[41,42] fit to the unit cell parameters.

The lattice strain $Q(hkl)$ was obtained directly from the linear relation between the observed d spacing and $(1 - 3\cos^2\psi)$ from Eq. (1). The ratio of differential to shear modulus, t/G, was evaluated from $Q(hkl)$ from Eq. (4) assuming $f = 1$. Figure 4 compares the increase of t/G with pressure of WB to that of other selected ceramics. t/G for WB first

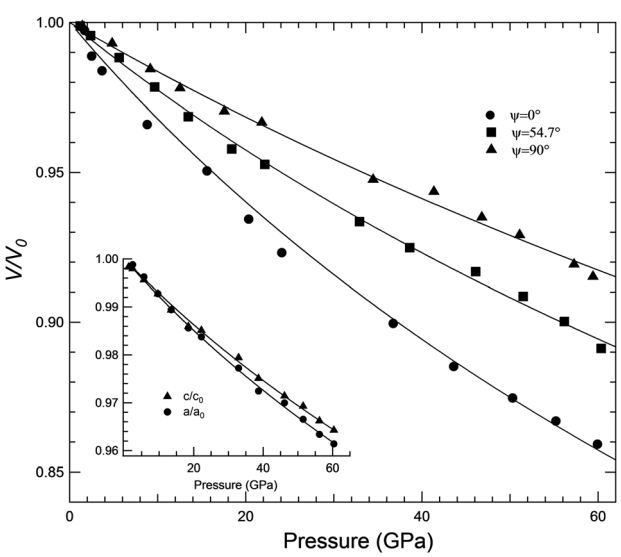

FIG. 3. Volumetric compression of WB measured at $\psi = 0°$, 54.7°, and 90°. The pressure is for each curve calculated from the measured diffraction data of W at the corresponding angle. The solid lines are Birch-Murnaghan equation fits to the data at each angle. Inset:Relative lattice parameters vs. pressure of WB. The solid lines are third-order Birch-Murnaghan equation of state fits to the relative unit cell parameters.

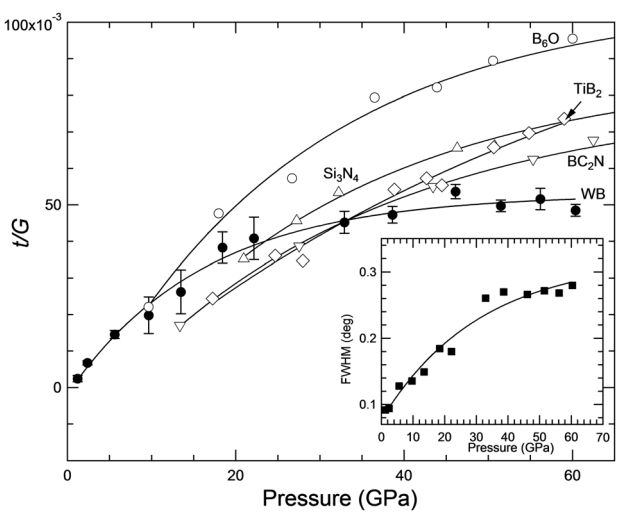

FIG. 4. Ratio of differential stress to aggregate shear modulus (t/G) of WB and selected ceramics[17,22,43,44] as a function of pressure. The inset is the average of full width at half-maximum (FWHM) of WB (004), (101), (103), (105), and (107) diffraction peaks at $\psi = 54.7°$. The solid lines are an exponential fit to the data.

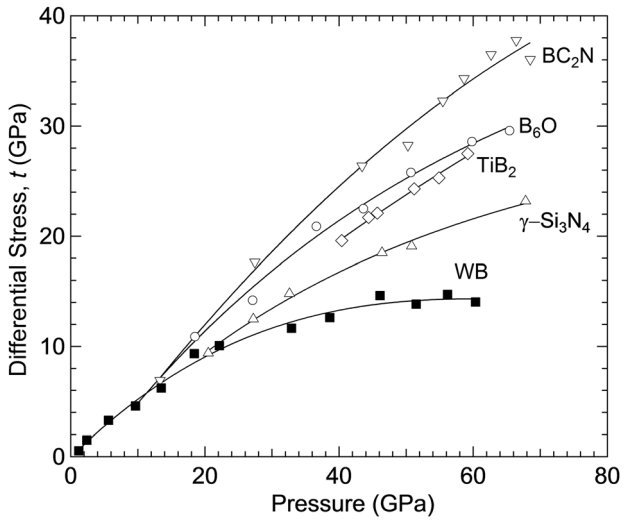

FIG. 5. Differential stress as a function of pressure. Solid squares: WB; Open symbols: other hard materials reported in the literature (▽: BC_2N,[44] ○: B_6O,[43] ◇: TiB_2,[17] Δ: γ-Si_3N_4 (Ref. 22)).

increases with pressure as differential stress builds in the sample, but then leve1s off and increases more slowly above ~20 GPa with a similar trend that is observed in the variation of the average FWHM (full width at half maximum) of WB diffraction lines with pressure (inset, Fig. 4). The broad diffraction peak widths of tungsten boride are due to the local deviatoric stresses among WB grains under nonhydrostatic compression as well as its nanostructure. Taken together, these observations indicate that WB starts to yield at ~20 GPa. At pressures of 40–60 GPa, the differential stress supported by WB is ~5% of the shear modulus, which is smaller than the values of other hard solids such as TiB_2, B_6O, c-BC_2N, and γ-Si_3N_4 (Fig. 4). These strong ceramics[17,22,43,44] achieve a value of $t/G \sim 8\%$–10% at the highest pressures. Thus, while WB is relatively incompressible, its strength is a smaller fraction of the shear modulus than that of other strong solids.

The aggregate shear modulus at high pressure was estimated by extrapolating the theoretically calculated ambient value[6] using an assumed pressure deviative, dG/dP, in the range of 1.0–1.5, which are typical values for ceramics.[45] This allows the differential stress of WB to be estimated as a function of pressure from Eq. (4) (Fig. 5). The maximum differential stress corresponds to the yield strength of the material once plastic deformation begins.[14] The yield strength of WB at 60.4 GPa is ~14 GPa. The supported differential stress of a number of hard materials with increasing pressure is also shown in Fig. 5. WB shows similar differential stress as other strong ceramics[17,22,43,44] below ~15 GPa. However, WB is much weaker compared to these strong solids at higher pressure.

CONCLUSIONS

The high pressure behavior of nanocrystalline tungsten boride (WB) has been investigated experimentally up to 60.4 GPa using radial x-ray diffraction techniques in a diamond anvil cell. The compression properties and stress state are analyzed using lattice strain theory. The *c* axis of WB is slightly more incompressible than the *a* axis. The hydrostatic compression curve at $\psi = 54.7°$ yields a bulk modulus of 417 GPa with a pressure derivative of 4.6. While these values are only semi-quantitative, they support recent density functional theory calculations that indicate the bulk modulus of WB is greater than 350 GPa, and thus it is a highly incompressible solid. Future measurements under hydrostatic or quasi-hydrostatic conditions are necessary to better constrain the bulk modulus. From the lattice stain anisotropy, a maximum differential stress of ~14 GPa is observed for WB at 60.4 GPa. This is about 5% of the value of the shear modulus at this pressure. At high pressures, WB is relatively weaker than other hard ceramics which can support differential stresses of ~8%–10% of the shear modulus at comparable pressures. Thus, while WB is highly incompressible, its strength is relatively low.

ACKNOWLEDGMENTS

We thank Z. Q. Chen and X. G. Hong of Stony Brook University for experimental assistance. This work was supported by the National Natural Science Foundation of China (Grant Nos. 11027405 and 10976018), China 973 Program (Grant No. 2011CB808200), and the Carnegie-DOE Alliance Center. Use of X17-C, National Synchrotron Light Sources was supported by COMPRES, the Consortium for Materials Properties Research in Earth Sciences under NSF Cooperative Agreement No. EAR EAR 10-43050, and by the U.S. Department of Energy, Office of Science, Office of Basic Energy Sciences under Contract No. DE-AC02-98CH10886.

[1]R. B. Kaner, J. J. Gilman, and S. H. Tolbert, Science **308**, 1268 (2005).
[2]R. W. Cumberland, M. B. Weinberger, J. J. Gilman, S. M. Clark, S. H. Tolbert, and R. B. Kaner, J. Am. Chem. Soc. **127**, 7264 (2005).
[3]Y. Chen, D. He, J. Qin, Z. Kou, S. Wang, and J. Wang, J. Mater. Res. **25**, 637 (2010).
[4]M. B. Weinberger, J. B. Levine, H. Y. Chung, R. W. Cumberland, H. I. Rasool, J. M. Yang, R. B. Kaner, and S. H. Tolbert, Chem. Mater. **21**, 1915 (2009).
[5]Y. Liang, X. Yuan, and W. Zhang, Phys. Rev. B **83**, 220102 (2011).
[6]E. Zhao, J. Meng, Y. Ma, and Z. Wu, Phys. Chem. Chem. Phys. **12**, 13158 (2010).
[7]R. Mohammadi, A. T. Lech, M. Xie, B. E. Weaver, M. T. Yeung, S. H. Tolbert, and R. B. Kaner, Proc. Natl. Acad. Sci. **108**, 10958 (2011).
[8]M. Xie, R. Mohammadi, Z. Mao, M. Armentrout, A. Kavner, R. Kaner, and S. Tolbert, Phys. Rev. B **85**, 064118 (2012).
[9]I. Frantzevitch, V. Lavrenko, and L. Glebov, Oxid. Met. **6**, 1 (1973).
[10]G. V. Samsonov, *Handbook of Refractory Compounds* (IFI/Plenum, New York, 1980).
[11]T. I. Serebryakova, V. A. Neronov, and P. D. Peshev, *High-Temperature Borides* (Cambridge Int. Sci. Publishing, Cambride, 2003).
[12]W. G. Fahrenholtz, G. E. Hilmas, I. G. Talmy, and J. A. Zaykoski, J. Am. Ceram. Soc. **90**, 1347 (2007).
[13]Y. Chen, D. He, J. Qin, Z. Kou, and Y. Bi, Int. J. Refract. Met. Hard Mater. **29**, 329 (2010).
[14]A. K. Singh, C. Balasingh, H.-K. Mao, R. J. Hemley, and J. Shu, J. Appl. Phys. **83**, 7567 (1998).
[15]T. S. Duffy, G. Shen, D. L. Heinz, J. Shu, Y. Ma, H.-K. Mao, R. J. Hemley, and A. K. Singh, Phys. Rev. B **60**, 15063 (1999).
[16]S. Merkel, H. R. Wenk, J. Shu, G. Shen, P. Gillet, H.-K. Mao, and R. J. Hemley, J. Geophys. Res. **107**, 2271 (2002).
[17]G. M. Amulele, M. H. Manghnani, and M. Somayazulu, J. Appl. Phys. **99**, 023522 (2006).
[18]A. K. Singh, J. Appl. Phys. **73**, 4278 (1993).
[19]A. K. Singh, H.-K. Mao, J. Shu, and R. J. Hemley, Phys. Rev. Lett. **80**, 2157 (1998).

[20]T. S. Duffy, G. Shen, J. Shu, H.-K. Mao, R. J. Hemley, and A. K. Singh, J. Appl. Phys. **86**, 6729 (1999).
[21]S. R. Shieh, T. S. Duffy, and B. Li, Phys. Rev. Lett. **89**, 255507 (2002).
[22]B. Kiefer, S. R. Shieh, T. S. Duffy, and T. Sekine, Phys. Rev. B **72**, 014102 (2005).
[23]A. K. Singh, J. Phys. Chem. Solids **65**, 1589 (2004).
[24]A. K. Singh, J. Appl. Phys. **106**, 043514 (2009).
[25]A. K. Singh and H. P. Liermann, J. Appl. Phys. **109**, 113539 (2011).
[26]A. Hammersley, S. Svensson, M. Hanfland, A. Fitch, and D. Häusermann, High Press. Res. **14**, 235 (1996).
[27]R. S. Hixson and J. N. Fritz, J. Appl. Phys. **71**, 1721 (1992).
[28]J. Z. Jiang, J. S. Olsen, L. Gerward, and S. Mørup, Europhys. Lett. **44**, 620 (1998).
[29]R. E. Miller and V. B. Shenoy, Nanotechnology **11**, 139 (2000).
[30]B. Palosz, E. Grzanka, S. Gierlotka, S. Stel'makh, R. Pielaszek, U. Bismayer, J. Neuefeind, T. Proffen, R. Von Dreele, and W. Palosz, Z. Kristallogr. **217**, 497 (2002).
[31]B. Palosz, E. Grzanka, S. Gierlotka, S. Stel'makh, R. Pielaszek, U. Bismayer, J. Neuefeind, H. Weber, and W. Palosz, Acta Phys. Pol. A **102**, 57 (2002).
[32]B. Palosz, S. Stel'makh, E. Grzanka, S. Gierlotka, R. Pielaszek, U. Bismayer, S. Werner, and W. Palosz, J. Phys.: Condens. Matter **16**, S353 (2004).
[33]V. B. Shenoy, Phys. Rev. B **71**, 094104 (2005).
[34]Z. Wang, Y. Zhao, D. Schiferl, C. S. Zha, R. T. Downs, and T. Sekine, Appl. Phys. Lett. **83**, 3174 (2003).
[35]B. Chen, D. Penwell, M. Kruger, A. Yue, and B. Fultz, J. Appl. Phys. **89**, 4794 (2001).
[36]Z. Wang, V. Pischedda, S. K. Saxena, and P. Lazor, Solid. State Commun. **121**, 275 (2002).
[37]B. Chen, D. Penwell, and M. B. Kruger, Solid State Commun. **115**, 191 (2000).
[38]H. Liu, J. Hu, J. Shu, D. Häusermann, and H.-K. Mao, Appl. Phys. Lett. **85**, 1973 (2004).
[39]D. J. Weidner, Y. Wang, and M. T. Vaughan, Geophys. Res. Lett. **21**, 753 (1994).
[40]N. Funamori, M. Funamori, R. Jeanloz, and N. Hamaya, J. Appl. Phys. **82**, 142 (1997).
[41]C. Meade and R. Jeanloz, Geophys. Res. Lett. **17**, 1157 (1990).
[42]X. Xia, D. J. Weidner, and H. Zhao, Am. Mineral. **83**, 68 (1998).
[43]D. He, S. R. Shieh, and T. S. Duffy, Phys. Rev. B **70**, 184121 (2004).
[44]H. Dong, D. He, T. S. Duffy, and Y. Zhao, Phys. Rev. B **79**, 014105 (2009).
[45]D. G. Isaak, "Elastic properties of minerals and planetary objects," *Handbook of Elastic Properties of Solids, Liquids, and Gases*, edited by M. Levy, H. Bass, R. Stern, and V. Keepens (Academic, San Diego, CA, 2001).